Proceedings of the 2023 International Conference on Machine Learning and Automation
DOI: 10.54254/2755-2721/30/20230075

Research on space attitude recognition and control method for soft robotics based on neural networks

Dahai Wang

Chongqing University, No.174 Shazheng Street, Shapingba District, Chongqing 400044, China

wang2dh@mail.uc.edu

Abstract. In the modern field of biomedical robotics, there is increasing attention on the use of soft robots as carriers for surgical devices. Compared to rigid robots, soft robots exhibit more complex postures and work environments, requiring new methods for recognizing and controlling their postures within biological organisms. This paper investigates the recognition and control of the posture of soft robots using a neural network learning approach, utilizing a soft robot equipped with resistive sensors. By establishing the relationship between changes in resistance values and posture variations, the study successfully achieves the identification and control of the soft robot's posture. The obtained posture data based on resistance values are validated for reliability. Thus, by combining resistive sensors with soft robots and employing neural network analysis, the recognition and control of soft robots' postures within biological organisms can be achieved.

Keywords: soft robotics, pneumatic drive, machine vision, flexible resistive sensor.

1. Introduction

With the ongoing development of minimally invasive surgical techniques, a new generation of minimally invasive surgical approaches is being developed with the goal of utilizing already existing biological pathways during operations. This will result in a reduction in the number of incisions required and a reduction in the risk of patient infection [1]. However, the majority of present surgical robotic arms are straight-arm robots that are made of multiple stiff materials and structures. Because of this, they are unable to move freely within the cavities of the human body without inflicting damage [2]. As a direct result of this, the concept of employing flexible robotic arms to carry surgical items has gained an increasing amount of attention. The complicated posture that flexible robotic arms maintain when they are in use is one of their defining characteristics. As a result, improved and more trustworthy methods of posture recognition are required.

Researchers are currently utilizing a variety of driving methods for soft robotics. These include fluid-based variable-pressure drive [3], smart material deformation drive [4], and internal combustion drive [5]. Pneumatic drive (Pneumatic drive means to use gas as a source of driving force for a robot) is the driving method that is employed the most frequently, however. Pneumatic drive is highly suitable in a wide variety of flexible mechanical constructions due to its simple and dependable structures, as well as its pollution-free characteristics, lightweight and widely available media, and other advantageous qualities [6].

DOI: 10.54254/2755-2721/30/20230075

When it comes to the self-perception of soft robot postures, the following types of sensors are frequently used: 1) Fiber Bragg Grating (FBG, FBG is a periodic structure in an optical fiber that reflects a specific wavelength of light) optical sensors, which utilize the principle of establishing the relationship between wavelength and strain, temperature, or curvature by inputting a specific narrow-range wavelength through a broadband reflective light source. As a result, these sensors are able to obtain the robot's status information and reconstruct its complex structure [7]. The reflected wavelength, on the other hand, is sensitive to strain, curvature, and temperature in the surrounding environment. 2) Electromagnetic (EM) and permanent magnet sensors. The spatial position information of the soft robot can be determined using EM sensors since they monitor changes in the electromagnetic field generated by the electromagnetic generator that is embedded in the driver [8]. This electromagnetic generator could be something like a micro magnet. Monitoring the changes in the magnetic field induced by variations in the position of the permanent magnet is another method that can be utilized to establish self-perception in a soft robot [9]. Although electromagnetic and permanent magnet sensors have benefits such as being small in size, having a high degree of precision, and being immune to interference from light, these sensors are prone to measurement errors because of interference from other medical devices' external magnetic fields. 3) Stress sensors that utilize capacitance and resistance. Resistance and capacitance sensors are the types of sensors that are used the most frequently because they monitor the deformation of the substrate by converting complex mechanical deformations into electrical signals. This makes them more extensively used than the preceding two types of sensors. In addition, as a result of the exceptional scalability of these materials, they show significant potential for use on soft and uneven surfaces, such as artificial skin and flexible actuators. Additionally, stretchable resistive and capacitive sensors are less difficult to build, have cheaper prices, are more easily integrated with soft actuators, and have a smaller impact on the deformation of the actuator [10].

In this article, we offer a method for detecting and controlling the posture of pneumatic chamber soft robots by merging neural network machine learning technology with resistive flexible sensors. This combination allows us to recognize and control the posture of the robots. Reading the feedback resistance value allows for real-time posture detection, which is made possible by the neural network's discovery of the association between resistance signals and actual postures, which was previously unknown. In this part of the research, the design and fabrication processes based on this system are investigated further, and a portion of the data that was collected is analyzed.

2. Soft actuator and flexible sensor design

In this study, a three-channel, multi-degree-of-freedom pneumatic soft actuator was chosen as the driving mechanism for this project. The main body of the actuator was cast from silicone rubber and externally wrapped with nylon fibers. Additionally, flexible resistive sensors utilizing multi-walled carbon nanotubes as conductive fillers and elastic silicone polymers as stretchable matrices were selected. These sensors exhibit advantages such as fast response time (~200ms), high force sensitivity (160-300mN), high stability, and the ability to withstand multiple cycles (1000 times).

2.1. Actuator design scheme

The designed pneumatic artificial muscle actuator in this study features a silicone rubber nylon fiber composite layer on the outside, with three chambers uniformly distributed along the 120° circumferential direction within the silicone rubber matrix, as shown in Figure 1(a). A central circular through-hole in the matrix serves as a pathway for minimally invasive surgical instruments, fixtures, and cameras. The actuator is sealed at both ends with end caps, which have air holes for the inflow of driving gas. To ensure stable adhesion between the end caps and the actuator, two inserts are designed near the air holes at the bottom of the end caps. The specific dimensional parameters are presented in Table 1.

DOI: 10.54254/2755-2721/30/20230075

Table 1. Actuator dimensional parameters.

Actuator Length L_1 /mm	Outer Diameter Φ_1 /mm	Inner Diameter Φ_2 /mm	External Diameter of the Drive Chambers Φ_3 /mm	Internal Diameter of the Actuator Φ_4 /mm	End Cap Length L_2 /mm	Insert Length L_3 /mm
80	16	8	13	11	5	3

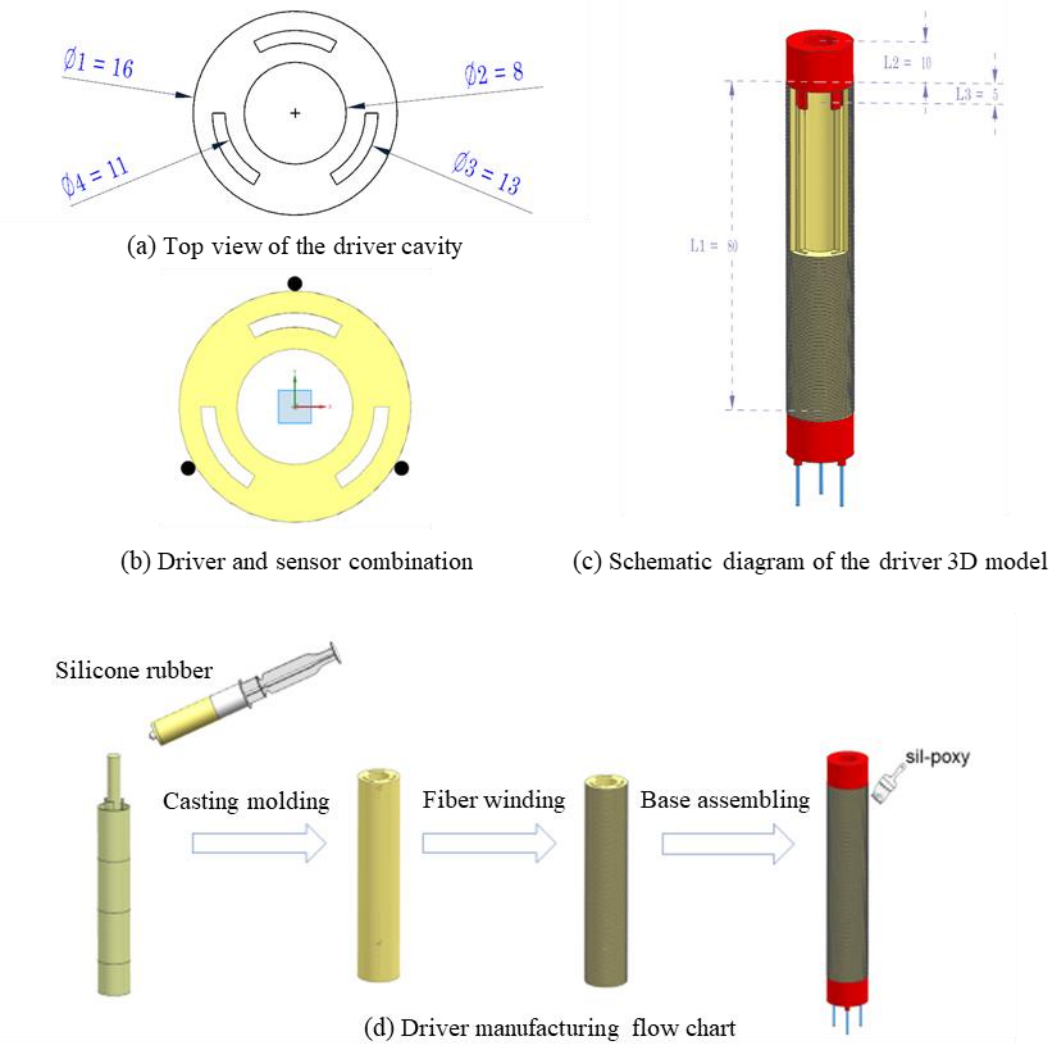

(a) Top view of the driver cavity

(b) Driver and sensor combination

(c) Schematic diagram of the driver 3D model

(d) Driver manufacturing flow chart

Figure 1. Actuator and sensor design and fabrication.

2.2. Actuator fabrication method

The following activities make up the primary procedure for producing the artificial pneumatic muscle actuator that will be used in this investigation. To begin, molds made of resin material were fabricated using 3D printing and then assembled. Gaps were then sealed using a hot glue gun in order to prevent silicone rubber liquid from leaking out of the molds. After that, the A and B components of the Ecoflex-0030 silicone rubber were combined in a ratio of 1:1, swirled in a mixer to get rid of any air bubbles, and then let to sit for later application. After the bubbles in the silicone rubber had been eliminated, the prepared silicone rubber was poured into the molds via the top cover of the mold, and the molds were then allowed to cure. After the silicone rubber had completely set, the molds had to be removed so that

DOI: 10.54254/2755-2721/30/20230075

the actuator could be demolded and retrieved. The end caps were made with 3D printing, and sil-poxy silicone adhesive was used to attach them to both ends of the actuator. At long last, nylon binding fibers were used to evenly wrap the actuator before being fastened in place with sil-poxy silicone adhesive. The creation of the artificial pneumatic muscle actuator is depicted in Figure 1(d), which shows the manufacturing process.

2.3. Sensor fabrication method

In this study, the conductive fillers for resistive-type flexible sensors were determined to be multi-walled carbon nanotubes (MWCNTs), while the stretchable matrices were determined to be elastic silicone polymers. The generation of electrical conductivity in multiwalled nanotubes is caused by the passage of electrons between the nanotubes. The amount of strain that is given to the sensor causes the space between the MWCNTs to rise, which in turn causes the electrical conductivity of the sensor to decrease while simultaneously increasing its total resistance. These sensors offer both great sensitivity and inexpensive manufacturing costs, making them an attractive option [11]. A distribution approach was established in order to meet the single mapping principle for precise sensor measurement. This strategy places the three chambers of the actuator, which are evenly distributed at 120° intervals along the circumferential direction, in close proximity to the actuator. The chambers are evenly spaced at 120° intervals along the circumferential direction. When the chambers are bent in this way, it is possible to collect data from each sensor. Figure 1(b) illustrates this point. In addition, as the inflation pressure rises, the flexible sensors experience stretching deformation, while at the same time the soft actuator experiences bending deformation. When the flexible sensors and the surface of the soft actuator are bent and deformed, embedding the sensors between the soft actuator and the nylon fiber binding layer helps avoid slippage between the flexible sensors and the surface of the soft actuator.

2.4. Signal acquisition circuit design

To real-time capture the resistance values of the resistive-type flexible sensors, a signal acquisition and processing system combining a microcontroller and a computer was employed in this study. When the spatial orientation of the actuator changes, the resistance values of the three resistive-type flexible sensors symmetrically distributed on the actuator correspondingly change. The scanning circuit of the resistive-type flexible sensors converts the resistance values into voltage signals. The microcontroller collects and performs analog-to-digital conversion on the voltage signals, while the computer receives the data collected by the microcontroller through a serial port, processes it, and displays and saves it. The signal acquisition system scheme used in this study is shown in the following diagram.

The scanning circuit for the three-channel resistive-type flexible sensors is the same. The circuit used in this project converts the resistance of one sensor into a voltage signal. The circuit mainly consists of a reference voltage, a resistor, and an operational amplifier. The reference voltage (VCC) is divided by the sensor resistor (R_x) and the reference resistor (R_ef) to obtain the voltage signal, which is then output after isolation by the operational amplifier. It is then amplified by a differential amplifier circuit and output to the ADC acquisition port of the Arduino after isolation by the operational amplifier. To minimize interference between sensing units during the scanning measurement process, a grounding resistor (R_5) is also connected at the reference voltage. The relationship between the output voltage (Vout) and the sensor resistance is given by the following equation:

$$Vout = \frac{R_{ef}}{R_x + R_{ef}} * VCC * 2 \tag{1}$$

3. Experimental method and results

3.1. Experimental platform setup

A closed-loop control system was used to regulate the behavior of the soft actuator, as can be seen in Figure 2. The Arduino control board received the control commands that were transmitted from a personal computer. In order to maintain a consistent air pressure throughout the system, the Arduino

DOI: 10.54254/2755-2721/30/20230075

control board, upon being given the instructions, modified the pin states in order to affect an adjustment to the pulse width modulation (PWM) duty cycle. Hoses were used to create connections between the air pump and the solenoid valves and the soft actuator, which made it possible for the gas to be supplied to the soft actuator. A pressure sensor was used to provide feedback to an Arduino control board in real time regarding the system's current air pressure. When the soft actuator's internal air pressure reached the target value, the personal computer instructed the Arduino control board to halt the relay by attaching a pin to the relay's IN signal. This was done so that the relay would no longer operate. This led to the closing of the solenoid valves and the stoppage of air inflation, which kept the soft actuator in the state it was in previously. Figure 3(a) depicts the actual wiring and hardware configuration of the control system.

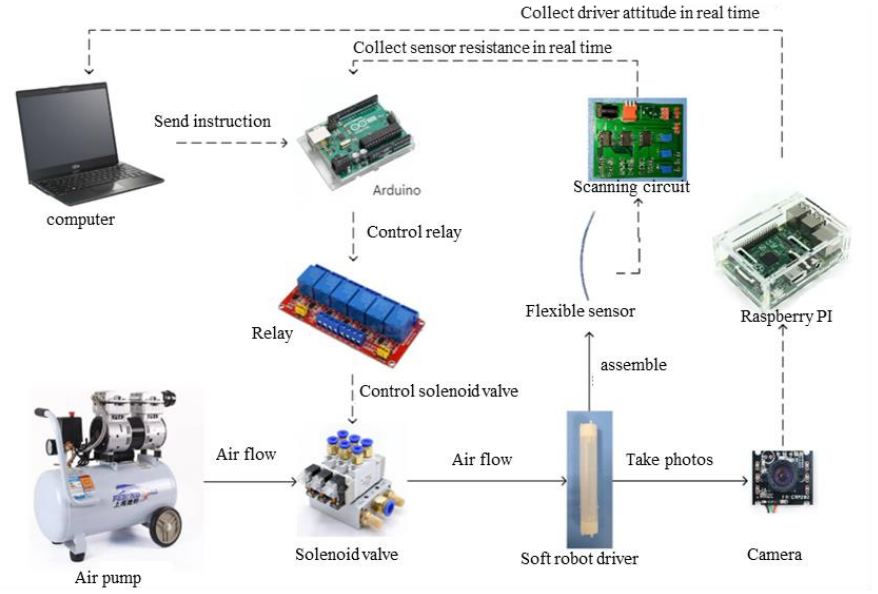

Figure 2. Overall control flow diagram.

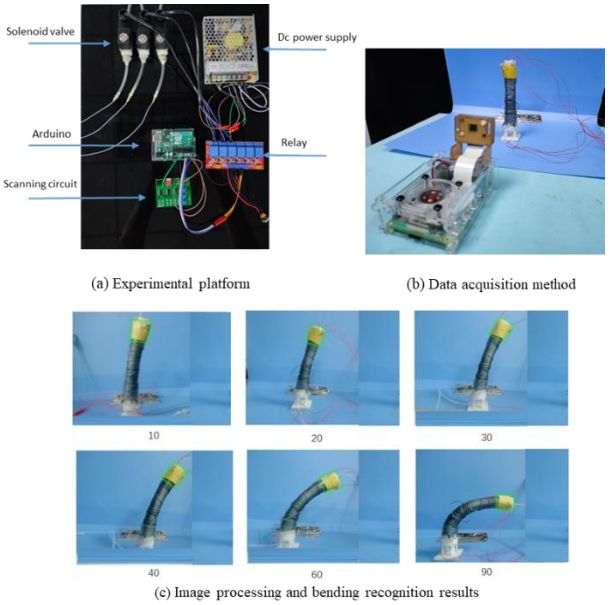

Figure 3. Experimental platform and results.

DOI: 10.54254/2755-2721/30/20230075

3.2. Soft robot pose acquisition

The bending deformation of the soft actuator target is a slow process, and the positional changes at the ends are continuous. Due to the relatively large size of the soft actuator in relation to the camera's field of view, a color-based detection method was employed for measuring the bending angles of the soft actuator. The collected data set was used for subsequent training.

Color markers were placed at the ends of the soft robot, and the soft robot was positioned in an artificial background under natural lighting conditions. A Raspberry Pi 4B was connected to an industrial camera, which was positioned directly in front of the soft actuator, capturing the color markers, as shown in Figure 3(b). To ensure sufficient detection accuracy, a 90-degree distortion-free industrial camera was selected, which provided a small field of view while effectively capturing the motion of the soft actuator. The main parameters of the camera are summarized in Table 2. Since the deformation of the soft robot units is slow and real-time requirements for the machine vision measurement system are not high, a Raspberry Pi was used as the platform for image processing and parameter extraction in the machine vision system. Once the soft actuator reached a certain bending angle, the Raspberry Pi controlled the camera to capture an image. Subsequently, OpenCV was utilized to process each frame of the captured images, extract the color target unit, and identify the bending angle of the soft actuator.

The first step of image processing involved the extraction of the target unit from the captured images using OpenCV. Gaussian filtering was applied to preprocess the images, blurring them and suppressing noise. The Gaussian filter function is expressed as:

$$G(x,y) = \frac{1}{2\pi\sigma^2} e^{-\frac{x^2+y^2}{2\sigma^2}} \tag{2}$$

In this expression, σ represents the standard deviation of the Gaussian distribution, and x and y represent the corresponding pixel coordinates. The cv2.cvtColor() command was used to convert the color space of the image to HSV style. The cv2.threshold() function was applied to remove the background and convert the image into a binary image for detection. The image was further eroded using cv2.erode() to remove noise. Finally, the contours of the color markers were identified, and rectangular bounding boxes were drawn. Figure 3(c) shows the results of the processed image, with the green bounding box indicating the detected position and angle of the color marker. After obtaining the graphical data, shape parameterization was performed. The bending angle of the soft robot is defined as the angle between the axis of the actuator and the vertical direction. Therefore, by extracting the contours of the color markers from the processed image and drawing rectangular bounding boxes, the bending angle of the soft robot can be calculated. Simple geometric calculations reveal that the bending angle θ of the soft robot is equal to the angle φ between the rectangular bounding box and the horizontal line. The size of φ can be calculated using the built-in functions of OpenCV, thereby obtaining the bending angle θ.

3.3. Neural network-based spatial pose analysis

In this study, a neural network approach was employed to learn the relationship between sensor data and the bending angles of soft actuators. To accomplish this, a backpropagation (BP) neural network was constructed using the TensorFlow framework. The BP neural network consisted of 15 hidden layers, and the softmax function was utilized as the activation function, defined as:

$$S_i = \frac{e^i}{\sum_j e^j} \tag{3}$$

In this expression, i and j represent the indices of the elements.

The learning rate of the model was set to 0.001, and the optimization algorithm chosen was stochastic gradient descent (SGD). The parameter update expression for SGD is as follows:

DOI: 10.54254/2755-2721/30/20230075

$$\theta^{(t)} \leftarrow \theta^{(t-1)} \leftarrow \varepsilon_t \frac{1}{B} \sum_{t'=Bt+1}^{B(t+1)} \frac{\partial L(z_{t'}, \theta)}{\partial \theta} \tag{4}$$

In this expression, B represents the size of the dataset, ε_t denotes the learning rate, θ represents the independent variable, t signifies the epoch number, and z represents the objective function.

In this study, the collected data consisted of the rate of resistance change of the flexible sensors and the bending angles of the soft robot in two scenarios: single-chamber loading and simultaneous dual-chamber loading. The rate of resistance change is calculated as:

$$\frac{R - R_0}{R_0} \tag{5}$$

In this expression, R_0 represents the initial resistance, and R represents the resistance after force application.

The data division for the two scenarios is presented in Table 3. For the single-chamber scenario, 200 sets of data were collected for each of the three chambers under different pressure conditions. For the dual-chamber scenario, 100 sets of data were collected for each combination.

Table 2. Data division table.

Number of Chambers	Total Data Count	Training Set Count	Test Set Count
1	600	480	120
2	300	240	60

For the single-chamber scenario, after training the BP neural network, the obtained model was used to predict the bending angles in the test set and compared with the ground truth values, as shown in Figures 3. It can be observed that the predicted bending angles in the test set closely match the ground truth values. The model's performance was evaluated using the mean absolute error (MAE), defined as:

$$MAE = \frac{1}{n} \sum_{n=1}^{i} |\hat{y}_i - y_i| \tag{6}$$

In this expression, n represents the total number of samples, $\hat{y}_i$ represents the sample mean value, and y represents the predicted values in the test set. The coefficient of determination (R^2) was calculated as follows:

$$r_{XY} = \frac{Cov(X, Y)}{S_X S_Y} \tag{7}$$

In this expression, Cov(X, Y) denotes the covariance between X and Y sets, and S_X, S_y represent the sample standard deviations of X and Y.

The root mean square error (RMSE) is mathematically expressed as:

$$RMSE = \sqrt{\frac{1}{m} \sum_{m}^{i=1} (y_i - \hat{y}_i)^2} \tag{8}$$

In this expression, M represents the number of sample points, $\hat{y}_i$ represents the sample mean value, and y represents the predicted values in the test set.

DOI: 10.54254/2755-2721/30/20230075

These metrics were utilized to assess the accuracy of the neural network model's predictions. Tables 4 and 5 present the MAE, R^2, and RMSE values obtained after training the single-chamber and dual-chamber models using the BP neural network.

Table 3. MAE, R^2, and RMSE of the single-chamber model obtained after training with the BP neural network.

Chamber Number	MAE	R^2	RMSE
1	0.75	0.966	0.92
2	1.45	0.973	1.09
3	1.1	0.919	0.94

Table 4. MAE, R^2, and RMSE of the dual-chamber model obtained after training with the BP neural network

Chamber Number	MAE	R^2	RMSE
1，2	1.18	0.933	0.99
2，3	1.28	0.906	1.37
1，3	1.09	0.956	0.86

The predicted results after learning for the single-chamber scenario are depicted in Figure 4, while the dual-chamber results are shown in Figure 5. In the graph illustrating the relationship between the rate of resistance change in the single-chamber scenario and the bending angle of the soft actuator, it can be observed that their relationship approximates a nonlinear smooth curve, facilitating network learning. However, in the case of applying pressure to both chambers simultaneously, their relationship forms a spatial trajectory. Due to the limited dataset and simplicity of the model in both scenarios, the training time was short, and the BP neural network algorithm yielded good predictive performance.

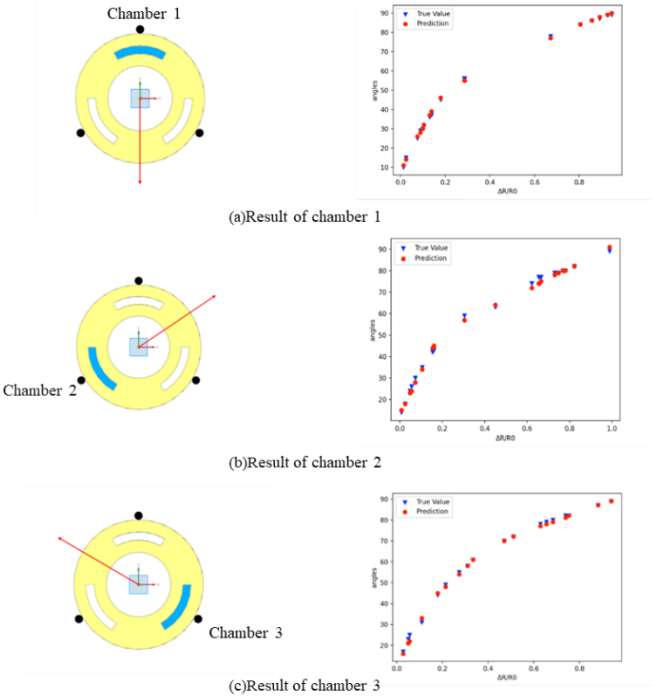

Figure 4. Predicted values versus ground truth values for the single-chamber drive.

DOI: 10.54254/2755-2721/30/20230075

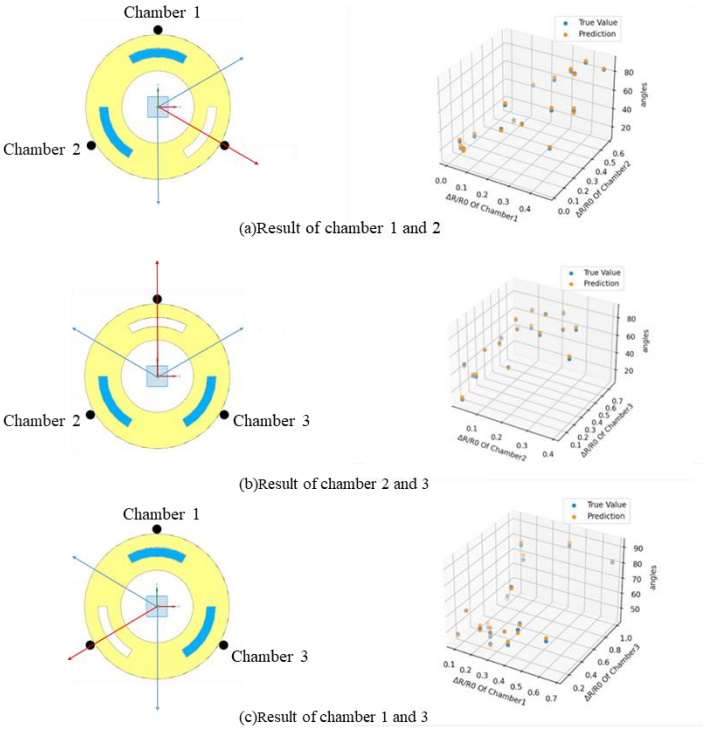

Figure 5. Predicted values versus ground truth values for simultaneous dual-chamber drive.

4. Discussion

In this study, we proposed a self-perception method for perceiving and predicting the three-dimensional spatial deformation of a multi-degree-of-freedom pneumatic soft robot. Our approach is based on the integration of three flexible resistive sensors with the soft actuators and the collection of the robot's deformation using computer vision. Subsequently, the resistive signals collected by the flexible sensors were fused into shape parameters of the soft robot using a BP neural network. These shape parameters can effectively predict the bending angles of the soft robot in three-dimensional space.

In the graph illustrating the relationship between the rate of resistance change in the single-chamber scenario and the bending angle of the soft actuator, it can be observed that their relationship approximates a nonlinear smooth curve, making it easy for the network to learn. By learning the relationship between the two through the neural network, it is possible to predict the deformation and bending of the actuator accurately. In the case of applying different pressures to both chambers simultaneously, their relationship forms a spatial trajectory. After learning through the neural network and fusing the data from the resistive sensors, it is also possible to predict the spatial position of the actuator.

There are limitations to this study. Firstly, the resistive flexible sensors used in this study have resistance rates that can vary with temperature and humidity. The experiments were conducted under room temperature conditions, but if the soft robot operates in environments with significant external variations, its self-perception system may be affected. Secondly, due to time constraints, the dataset collected in this study was relatively small. Therefore, a BP neural network, suitable for smaller-scale datasets and relatively simple, was employed for data fitting. In future research, larger datasets can be collected, and more complex and high-precision neural network architectures can be utilized. Footnotes

Footnotes should be avoided whenever possible. If required they should be used only for brief notes that do not fit conveniently into the text.

DOI: 10.54254/2755-2721/30/20230075

5. Conclusion

By combining neural network-based data analysis techniques with the integration of silicon rubber soft robots and resistive flexible sensors, we analyzed the deformation and resistance values of the soft robot, uncovering underlying patterns. In both the single-chamber and multi-chamber pneumatic scenarios, the predicted deformation values obtained through the neural network were close to the measured values, with MAE, R^2, and RMSE falling within an acceptable range. This integration of analytical methods and hardware facilitates the detection of the posture of soft robots operating in environments where visual observation is not feasible. For example, in the case of surgical robots inside the human body, this method can be employed for posture assessment, contributing to improved operational precision and safety.

References

[1] Li, Z., Wang, G., Tan, J., et al. (2015). NOTES instrument workspace and human-machine interface: Concept, research status, and technological prospects. World Journal of Composite Materials, 1(4), 304-311.

[2] Wang, S., Wang, X., Zhang, J., et al. (2011). A new robot “Miao Shou A” for assisting laparoscopic surgery. Robot Technology and Application, (4), 17-21.

[3] Li, T., Li, G., Liang, Y., et al. (2016). Overview of research on structure mechanism and driving materials of soft robots. Acta Mechanica Sinica, 48(4), 756-766.

[4] Wang, Y., Ru, J., Zhao, D., et al. (2017). Research progress on electrode interface of ionic polymer-metal composites (IPMCs). Materials Reports, 31(15), 24-29.

[5] Bartlett, N. W., Tolley, M. T., Overvelde, J. T., et al. (2015). A 3D-printed, functionally graded soft robot powered by combustion. Science, 349(6244), 161-165.

[6] Wang, T., Hao, Y., Yang, X., et al. (2017). Soft robots: Structure, driving, sensing, and control. Journal of Mechanical Engineering, 53(13), 1-13.

[7] Xiong, L., Jiang, G., Guo, Y., & Liu, H. (2018). A three-dimensional fiber Bragg grating force sensor for robots. IEEE Sensors Journal, 18(9), 3632-3639.

[8] Tully, S., & Choset, H. (2016). A filtering approach for image-guided surgery with a highly articulated surgical snake robot. IEEE Transactions on Biomedical Engineering, 63(2), 392-402. https://doi.org/10.1109/TBME.2015.2461531.

[9] Guo, H., Ju, F., Cao, Y., Qi, F., Bai, D., Wang, Y., & Chen, B. (2019). Continuum robot shape estimation using permanent magnets and magnetic sensors. Sensors and Actuators A: Physical, 285, 519-530. ISSN 0924-4247.

[10] Tang, Z., Jia, S., Shi, X., Li, B., & Zhou, C. (2019). Coaxial printing of silicone elastomer composite fibers for stretchable and wearable piezoresistive sensors. Polymers, 11, 666.

[11] So, J., Kim, U., Kim, Y. B., et al. (2021). Shape estimation of soft manipulator using stretchable sensor. Cyborg and Bionic Systems, 2021.